






PAPER

[View Article Online](#)
[View Journal](#) | [View Issue](#)Cite this: *Dalton Trans.*, 2025, **54**,
10246

Chiral CNN pincer Ir(III)–H complexes. Transient ligand and counterion influences in the asymmetric hydrogenation of imines and quinolines†

Yisong Wen, ^{a,b} Albert Cabré, ^a Jordi Benet-Buchholz, ^c Antoni Riera ^{*a,b}
and Xavier Verdaguer ^{*a,b}

Building upon the success of Ir-IMMAX catalysts, we designed a novel cationic Ir(III)–H catalyst featuring a meridional CNN pincer ligand with a perpendicular monodentate phosphine, where chirality arises from both the chiral oxazoline moiety and the metal center itself. The catalyst is readily synthesized from commercially available precursors, obtained as a single diastereomer, and exhibits high activity in the asymmetric hydrogenation of imines and quinolines under mild conditions. One of the synthesized Ir(III)–H complexes efficiently reduced *N*-methyldimines and 2-methylquinoline at room temperature under 3 bar of H₂ pressure, positioning itself among the most active catalysts described to date. The incorporation of a weakly coordinating transient ligand, such as acetonitrile, significantly enhanced catalytic performance. Additionally, the counterion displayed an important influence on both enantioselectivity and activity, with the BARf complex providing higher selectivity and the triflate complex exhibiting superior reactivity.

Received 19th March 2025,
Accepted 26th May 2025

DOI: 10.1039/d5dt00667h

rsc.li/dalton

Introduction

Asymmetric hydrogenation (AH) is an essential method in modern synthetic chemistry, providing an efficient approach to enantiomerically enriched pharmaceuticals, agrochemicals and fine chemicals.¹ Iridium has been one of the most extensively studied transition metals for this application, since it provides highly active catalysts for the hydrogenation of challenging substrates such as non-functionalized alkenes, imines and nitrogen containing heteroaromatic compounds.^{2–7} In 2016, our group introduced a library of Ir-MaxPHOX catalysts featuring a *P*-stereogenic phosphino-oxazoline ligand (Fig. 1a), which have been successfully applied to the hydrogenation of both functionalized and non-functionalized alkenes.^{8–11} Building upon this foundation, we developed the Ir-IMMAX catalyst—an octahedral

Ir(III) hydride complex featuring a MaxPHOX ligand, a cyclometallated imine, and a transient solvent ligand.¹² The Ir-IMMAX catalyst has demonstrated outstanding efficiency and selectivity in the asymmetric hydrogenation of *N*-methyl, *N*-alkyl, and *N*-aryl imines, providing enantiomeric excesses (ee) of up to 99% under low hydrogen pressure (3 bar).¹³

Given the selectivity and efficiency achieved with the Ir-IMMAX catalyst in the hydrogenation of imines, we aimed to find alternative octahedral Ir(III) systems with comparable structural frameworks that allow straightforward synthesis, easier structural modification and larger reaction scope. This idea led us to explore the iridium pincer complexes, which have gained significant attention over the past decades due to their high modularity and exceptional stability.¹⁴ The first application of iridium pincer complexes was reported by Jensen, Kaska, and co-workers in 1996 for the transfer dehydrogenation of alkanes.¹⁵ Since then, many pincer complexes have been developed by fine-tuning various aspects of the ligand structure. However, their applications have predominantly focused on achiral transformations such as dehydrogenation, dehydroaromatization, and isomerization. In contrast, only a limited number of asymmetric transformations have been reported, with selected examples shown in Fig. 1b.^{16–20}

With the idea to mimic the coordination environment of the Ir-IMMAX complexes with a pincer ligand, we designed complex **A** (Fig. 1c), a cationic Ir(III) species featuring a meri-

^aInstitute for Research in Biomedicine (IRB Barcelona), The Barcelona Institute of Science and Technology, Baldori Reixac 10, Barcelona E-08028, Spain.

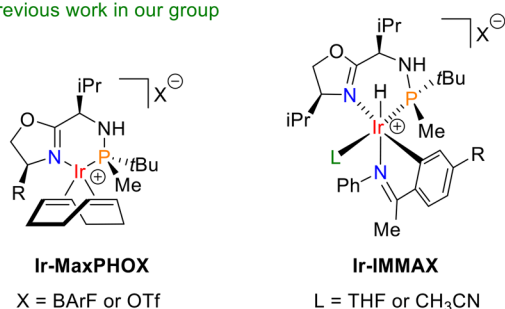
E-mail: xavier.verdaguer@irbbarcelona.org, antoni.riera@irbbarcelona.org

^bDepartament de Química Inorgànica i Orgànica, Secció de Química Orgànica, Universitat de Barcelona, Martí i Franquès 1, Barcelona E-08028, Spain

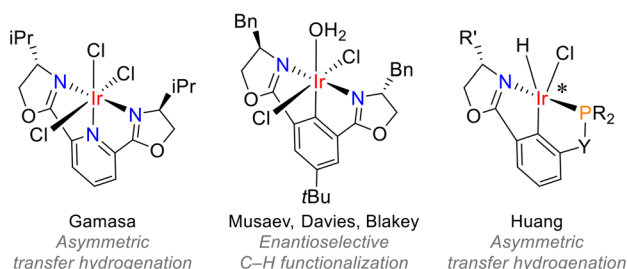
^cInstitute of Chemical Research of Catalonia (ICIQ), The Barcelona Institute of Science and Technology, Av. Països Catalans 16, 43007 Tarragona, Spain

†Electronic supplementary information (ESI) available: HPLC/GC methods, chromatograms, NMR spectra and X-ray crystallographic data. CCDC 2430455 and 2430460. For ESI and crystallographic data in CIF or other electronic format see DOI: <https://doi.org/10.1039/d5dt00667h>

a) Previous work in our group



b) Iridium pincer catalysts for asymmetric transformations



c) Present work



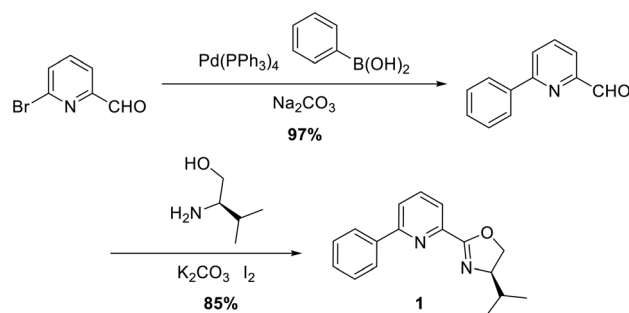
Fig. 1 Reported Ir-MaxPHOX and Ir-IMMAX catalysts, examples of iridium pincer catalysts for asymmetric transformations and the designed CNN pincer Ir(III)–H complex.

dional phenyl-pyridine-oxazoline pincer ligand, and a monodentate phosphine positioned perpendicular to the pincer plane. We anticipated that the phosphine would be placed *anti* relative to the oxazoline's isopropyl group, and that the transient ligand (L) would occupy the position *trans* to the phosphine, as observed in Ir-IMMAX complexes.

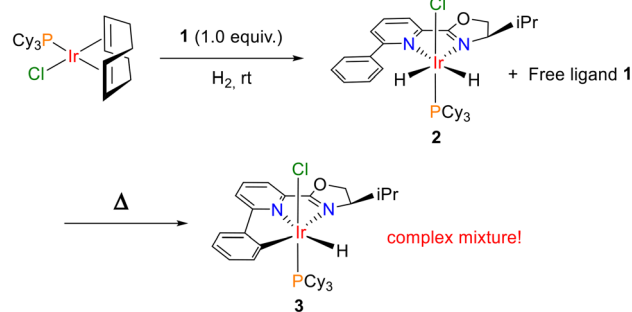
Here, we report the highly stereoselective, one-step synthesis of complexes **A** (X = OTf and BArF) with different transient ligands from readily available metal precursors. The structure of **A** and its dihydride synthetic intermediate has been unambiguously confirmed by single-crystal X-ray diffraction. The resulting complexes have been tested in the asymmetric hydrogenation of imines and quinolines, with the results highlighting the strong influence of both the transient ligand and counterion on the performance of the catalysts.

Results and discussion

Starting from 6-bromopicolinaldehyde, the model pincer ligand **1** was readily synthesized following a two-step procedure from available literature in high yield (Scheme 1).^{21,22} With the ligand in hand, initial attempts to synthesize the designed complex **A**



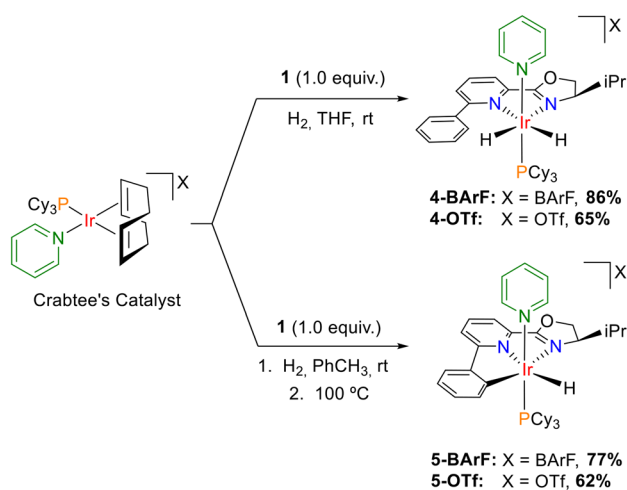
Scheme 1 Synthesis of CNN pincer ligand **1**.



Scheme 2 Initial attempts to synthesize the desired Ir(III) hydride CNN pincer complex.

started from the Ir(cod)(PCy₃)Cl (cod = 1,5-cyclooctadiene) precursor. We envisioned that removal of cod ligand by means of hydrogen and complexation with **1** would provide dihydride complex **2**, which upon heating would lead to cyclometallated complex **3** (Scheme 2). Chloride complex **3** would be a convenient precursor of the desired final complex since halogen abstraction would allow the generation of the desired vacant coordination site, which could be stabilized with a transient solvent ligand (*i.e.* THF or ACN). To this end, ligand **1** was added to the Ir precursor and cod was removed *via* hydrogen bubbling. ¹H NMR analysis of the reaction mixture revealed two doublets of doublets at –21.89 and –25.05 ppm suggesting that the corresponding dihydride **2** was obtained as major metal hydride species, along with substantial amounts (40–50%) of free starting ligand. Upon subsequent thermally induced cyclometallation (toluene, 100 °C), multiple hydride-containing products were observed from which the desired complex could not be isolated. More critically, we observed increased amounts of uncoordinated ligand post-cyclometallation, suggesting that the dihydride **2** was inherently unstable. This instability likely arises from the *N,N*-bidentate ligand adopting a *trans* arrangement relative to the two hydrides, making it prone to dissociation. An additional potential problem when using non-symmetric pincer ligands as **1** is the formation of different stereoisomers since the metal becomes a chiral center itself, as happens, for instance, in Huang's iridium complexes (Fig. 1b).¹⁹ Overall, we believed these factors were responsible for the inefficient synthesis of **3**.

Recognizing the need for improved stability and selectivity, we sought an alternative approach using a cationic precursor instead of a neutral one. We reasoned that a cationic complex, being more electrophilic, should provide increased stability to the corresponding dihydride intermediates. With this idea in mind, we turned our attention to Crabtree's catalysts. Starting from the BArF analogue of Crabtree's catalyst, ligand **1** was successfully coordinated following cod removal under hydrogen in THF at room temperature, yielding the dihydride intermediate **4-BArF** in significantly improved purity as a single diastereomer (Scheme 3). Notably, this intermediate exhibited sufficient stability to allow purification *via* column chromatography, affording a crystalline orange solid in 86% yield. In the $^1\text{H-NMR}$ spectrum (Fig. 2), the two hydrides appear as doublet of doublets at -21.00 ppm and -24.13 ppm, with a $J(\text{H,P})$ of 23.4 Hz and a $J(\text{H,H})$ of 8.2 Hz, confirming that both hydrides are located *cis* to the phosphorous atom.



Scheme 3 Synthesis of complexes **4** and **5** from the corresponding Crabtree's catalyst.

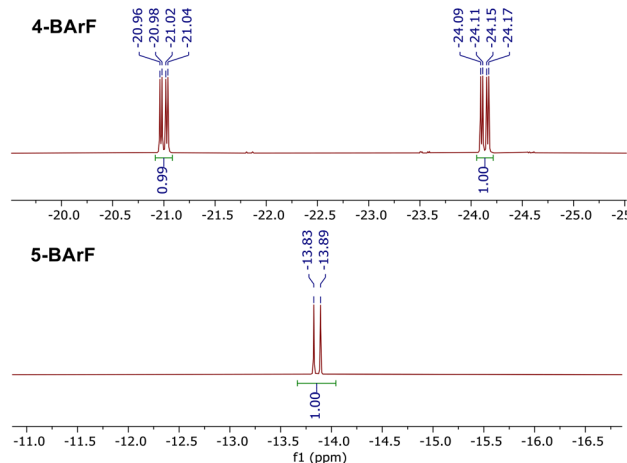


Fig. 2 Hydride zone in the $^1\text{H-NMR}$ spectra of **4-BArF** and **5-BArF**.

Performing the cod ligand removal in toluene at room temperature and subsequently heating to 100°C induced cyclometallation, producing the desired cyclometallated complex **5-BArF** in high purity and selectivity (Scheme 3). Again, column chromatography provided complex **5-BArF** as a crystalline orange solid in 77% yield. In the $^1\text{H-NMR}$ spectrum, the hydride appears as a doublet at -13.86 ppm, with a $J(\text{H,P})$ of 26.2 Hz, characteristic of a hydride *cis* to phosphorous atom (Fig. 2). A similar strategy was employed to synthesize the triflate analogues of both complexes (**4-OTf** and **5-OTf**, respectively), starting from the triflate analogue of Crabtree's catalyst.

Single-crystal X-ray structures of complexes **4-BArF** and **5-BArF** are depicted in Fig. 3. As hypothesized, the introduction of a bulky phosphine ligand such as tricyclohexylphosphine resulted in the formation of a single diastereomer for both complexes, with the phosphine positioned *trans* to the directing isopropyl group of the chiral oxazoline and perpendicular to the ligand plane. The bidentate ligand is confirmed to be *trans* to two hydrides in **4-BArF**, justifying the relatively low stability of this dihydride intermediate. In **5-BArF**, cyclometallation occurred with the release of a hydrogen molecule, leaving the remaining hydride positioned *trans* to the pyridine

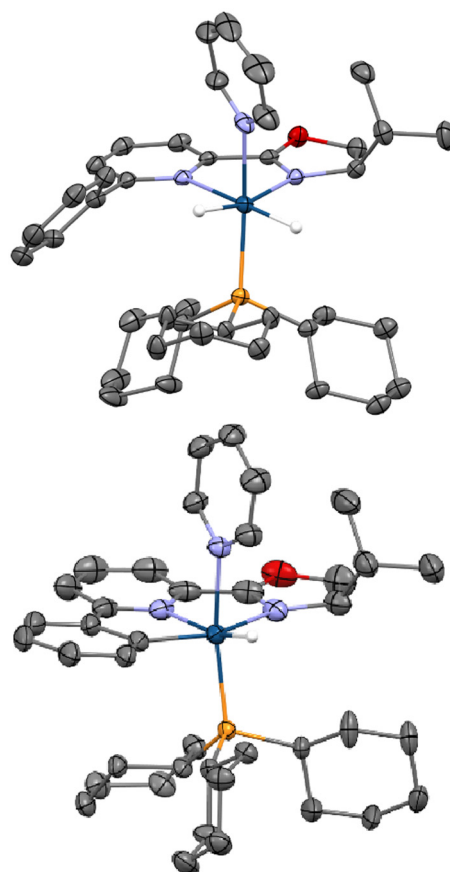


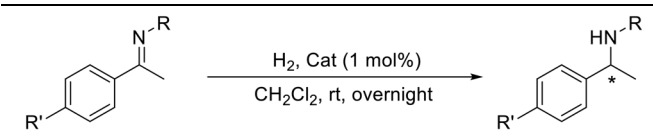
Fig. 3 Single-crystal X-ray structure of **4-BArF** (top) and **5-BArF** (bottom). The Ortep diagram shows ellipsoids at 50% probability. The BArF counterions and solvent molecules are omitted for clarity. Only the hydrides attached to the iridium center are shown.

moiety of ligand **1**. The reactive site is occupied by the coordinated pyridine, situated *trans* to the monodentate phosphine.

With these complexes in hand, we next sought to replace the coordinated pyridine with acetonitrile, a weaker and more labile transient ligand, mirroring the ligand environment of the Ir-IMMAX catalyst, as the acetonitrile ligand would likely enhance catalyst activity. Initially, direct synthesis from the corresponding acetonitrile analogue of Crabtree's catalyst, [Ir(CH₃CN)(cod)(PCy₃)]BARF, was attempted following the successful synthesis of **5-BArF** and **5-OTf**. However, such a strategy proved unfeasible due to the lower stability of the acetonitrile dihydride intermediate, leading to intricate mixtures of iridium hydride species. Finally, we sought the direct pyridine-acetonitrile ligand exchange on complex **5-OTf** (Scheme 4). Upon heating **5-OTf** in acetonitrile, a new doublet appeared at -15.24 ppm corresponding to the acetonitrile ligand exchange product **6-OTf**. Upon co-distillation of the outcoming pyridine with acetonitrile several times ($\times 3$), we could completely remove the pyridine to obtain the target **6-OTf**. Purification *via* flash chromatography provided the new complex in 71% yield and 92% purity, as determined by ¹H NMR.²³ At this point we proceeded to test the newly obtained species **4**, **5** and **6** as catalysts in AH.

To evaluate the catalytic performance of our synthesized complexes, we first investigated their activity and selectivity in the AH of imines (Table 1). As representative substrates, we selected 4-methoxy-substituted *N*-phenyl imine and 4-chloro-substituted *N*-methyl imine, owing to their enhanced stability and ease of handling as solids at room temperature. Hydrogenation was carried out at 1 mol% catalyst loading, using 50 bar and 3 bar of hydrogen pressure at room temperature in dichloromethane. Comparative analysis of conversions revealed that the dihydride complex **4-OTf** was the least active catalyst, likely due to its inherent instability leading to rapid deactivation. In contrast, all the cyclometallated catalysts provided full conversion at 50 bar of hydrogen with both substrates (Table 1, entries 5, 6, 9, 10, 13 and 14). Surprisingly, at a lower hydrogen pressure of 3 bar, the acetonitrile complex **6-OTf** was still able to provide full conversion for the hydrogenation of *N*-methyl imines (Table 1, entry 16). This is particularly notable, as reports of this transformation under such mild conditions are scarce, since *N*-methyl imines are challenging substrates due to the high nucleophilicity of the resulting

Table 1 Evaluation of synthesized complexes in the AH of acyclic imines



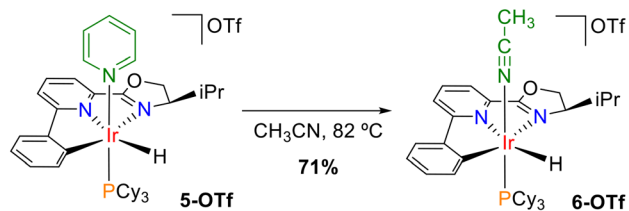
Entry	Catalyst	R, R'	H ₂ (bar)	Conv. ^a (%)	ee. ^b (%)
1	4-OTf	Ph, OMe	50	68	13 (<i>S</i>)
2	4-OTf	Me, Cl	50	30	—
3	4-OTf	Ph, OMe	3	0	—
4	4-OTf	Me, Cl	3	0	—
5	5-BArF	Ph, OMe	50	100	48 (<i>R</i>)
6	5-BArF	Me, Cl	50	100	89 (<i>R</i>)
7	5-BArF	Ph, OMe	3	60	48 (<i>R</i>)
8	5-BArF	Me, Cl	3	16	—
9	5-OTf	Ph, OMe	50	100	16 (<i>S</i>)
10	5-OTf	Me, Cl	50	100	48 (<i>R</i>)
11	5-OTf	Ph, OMe	3	100	19 (<i>S</i>)
12	5-OTf	Me, Cl	3	34	—
13	6-OTf	Ph, OMe	50	100	16 (<i>S</i>)
14	6-OTf	Me, Cl	50	100	45 (<i>R</i>)
15	6-OTf	Ph, OMe	3	100	17 (<i>S</i>)
16	6-OTf	Me, Cl	3	100	47 (<i>R</i>)

^a Conversion rate was determined *via* ¹H-NMR. ^b Enantiomeric excesses were determined *via* chiral HPLC/GC.

amine product, which tends to coordinate to the catalyst causing deactivation.²⁴ The superior reactivity of the acetonitrile-ligated complex supports our hypothesis that a weaker transient ligand enhances catalytic performance, whereas the corresponding pyridine-ligated complex exhibited lower conversion under identical conditions (Table 1, entry 12).

Interestingly, we observed a pronounced effect of the counterion on both selectivity and activity. Specifically, the cyclometallated complex **5-BArF** provided significantly higher enantioselectivity towards the (*R*)-enantiomer with up to 89% ee in the reduction of *N*-methyl imine (Table 1, entry 6); compared to **5-OTf** which afforded only 48% ee (Table 1, entry 10). In contrast, the triflate analogue **5-OTf** exhibited increased catalytic activity (Table 1, entries 7 *vs.* 11). This discrepancy could be rationalized by considering the potential involvement of the triflate anion in the transition state through hydrogen bonding interactions, as reported by Fan, Yu and co-workers,²⁵ which may stabilize a lower-energy transition state and thus enhance conversion. However, this interaction appears to stabilize the transition state leading to the (*S*)-enantiomer, as evidenced by the lower enantioselectivity observed for *N*-methyl imine (Table 1, entries 6 *vs.* 10) and the shift in selectivity toward the (*S*)-enantiomer in the case of *N*-phenyl imine (Table 1, entries 5 *vs.* 9). Finally, it is worth noting that enantioselectivity was nearly identical between the pyridine (**5-OTf**) and acetonitrile (**6-OTf**) variants (Table 1, entries 9–11 *vs.* 13–15). This fact aligns with the expectation that the dissociation of the transient ligand occurs before the catalytic cycle begins.

It has been proposed that the AH of imines catalyzed by cationic octahedral Ir(III) complexes follows an outer-sphere mechanism,²⁶ and a plausible catalytic cycle for the reduction



Scheme 4 Displacement of pyridine with acetonitrile to form complex **6-OTf**.

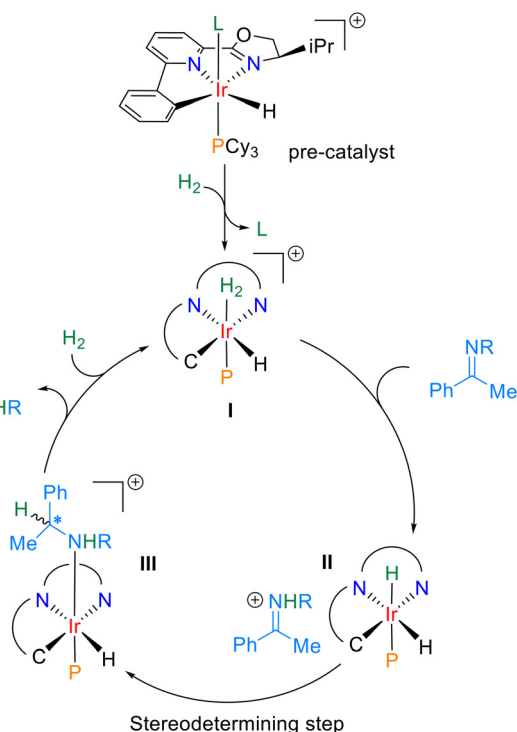


Fig. 4 Hydrogenation mechanism with Ir(III) octahedral catalysts.

of imines with catalysts 5–6 is depicted in Fig. 4. The transient ligand of the pre-catalyst is exchanged with a dihydrogen molecule leading to the active catalyst **I**. Subsequent activation of the imine substrate through protonation by the acidic Ir(III) dihydrogen complex **I** leads to the neutral dihydride **II** and the corresponding iminium ion. The stereodetermining step is the transfer of the hydride *trans* to the phosphine in **II** to the protonated substrate. For complexes **5-OTf** and **6-OTf**, we believe the activated iminium ion is H-bonded to the triflate counterion, which impacts both activity and selectivity of the system.

The catalytic activity of the synthesized complexes was then tested with 2-methylquinoline and 2-phenylquinoline (Table 2). The AH of heteroaromatic substrates is less explored than that of prochiral imines, primarily due to the increased stability imparted by the aromaticity of these compounds, which may require harsher reaction conditions.^{3,4} The AH of quinolines is thought to follow an outer-sphere mechanism as in the case of imines, although it proceeds through a cascade reaction pathway.²⁵ The AH of quinolines was carried out under identical conditions to those used for the imine substrates at 1 mol% catalyst loading in dichloromethane. Overall, the conversion data in Table 2 confirms that quinolines are more difficult to hydrogenate, with the 2-methylquinoline being easier to reduce than the phenyl substituted counterpart. With respect to the activity of catalysts 4–6, a similar trend is observed, with dihydride **4-OTf** providing very low conversions (Table 2, entries 1–4). Among the cyclometallated pyridine complexes, **5-OTf** demonstrated higher activity than the corresponding **5-BArF** counterpart (Table 2, entries 9–11 vs.

Table 2 Evaluation of synthesized complexes in the AH of quinolines

Entry	Catalyst	R	H ₂ (bar)	Conv. ^a (%)	ee. ^b (%)
1	4-OTf	Me	50	23	—
2	4-OTf	Ph	50	10	—
3	4-OTf	Me	3	0	—
4	4-OTf	Ph	3	0	—
5	5-BArF	Me	50	43	—
6	5-BArF	Ph	50	<5	—
7	5-BArF	Me	3	<5	—
8	5-BArF	Ph	3	0	—
9	5-OTf	Me	50	100	18
10	5-OTf	Ph	50	81	15
11	5-OTf	Me	3	25	—
12	5-OTf	Ph	3	<5	—
13	6-OTf	Me	50	100	19
14	6-OTf	Ph	50	100	12
15	6-OTf	Me	3	100	0
16	6-OTf	Ph	3	77	0

^a Conversion rate was determined via ¹H-NMR. ^b Enantiomeric excesses were determined via chiral HPLC.

5–7). A major reactivity difference was observed when changing the transient ligand from pyridine to acetonitrile. Full conversions were obtained for both quinolines at 50 bar of hydrogen pressure using **6-OTf** (Table 2, entries 13 and 14). Most notably, at 3 bar of hydrogen, 2-methyl and 2-phenylquinoline were reduced with 100% and 77% conversion respectively (Table 2, entries 15 and 16). Catalyst **6-OTf** is more active than the ruthenium catalyst described by Fan, Yu and co-workers,²⁵ and compares favorably with the achiral diphosphine-carbene iridium complex described by Crabtree and co-workers, which hydrogenates quinolines at 1 bar of H₂ pressure.²⁷ Hence, **6-OTf** is among the most active catalysts described in the literature for the reduction of quinolines. Unfortunately, the selectivity is very low and only 19% ee is obtained for the reduction of 2-methylquinoline (Table 2, entry 13). In this regard, we believe the selectivity could be improved by introducing secondary interactions (*i.e.*, H-bonding) between the substrate and the ligand structure like we recently demonstrated with the IMMAX catalyst system in the hydrogenation of imines.¹³

Conclusions

In summary, we have developed a novel octahedral Ir(III)–H catalyst featuring a meridional CNN pincer ligand with a monodentate phosphine positioned perpendicular to the pincer plane. The catalyst was readily synthesized as a single diastereomer with its structure confirmed by single-crystal X-ray diffraction, revealing its unique chiral environment derived from both the chiral oxazoline moiety and the metal center itself.

Evaluation of the catalysts in the AH of imines and quinolines demonstrated high activity under mild conditions.

Catalyst **6-OTf** was able to completely reduce *N*-methylamine and 2-methylquinoline at room temperature under 3 bar of H₂ pressure, positioning itself among the most active catalysts described to date. The presence of a weakly coordinating transient ligand, such as acetonitrile, significantly enhanced catalytic performance compared to the pyridine-ligated analogue. Additionally, counterions played a crucial role in both enantioselectivity and activity, with the triflate complex exhibiting superior reactivity, but lower enantioselectivity.

These results show that the novel iridium pincer-phosphine system can provide highly active catalysts, providing valuable insights for the rational design of next-generation iridium catalysts for asymmetric hydrogenation.

Experimental section

General methods

All reactions were carried out under nitrogen atmosphere in dried solvents. THF and CH₂Cl₂ were dried with PureSolv purification system from Innovative Technology, Inc. Other commercially available anhydrous solvents were used with no further purification. Silica gel chromatography was performed by using 35–70 mm silica and flash chromatography was performed on automated Combiflash® system from Teledyne Isco. NMR spectra were recorded at 23 °C on Varian Mercury 400 apparatus, with spectra referenced to the residual solvent peak. IR spectra were recorded with Thermo Nicolet Nexus FT-IR apparatus. HRMS were recorded in LTQ-FT Ultra (Thermo Scientific) using Nanoelectrospray technique. HPLC chromatography was performed on Agilent Technologies Series 1100 chromatograph with UV detector. GC chromatography was performed on Agilent Technologies 6890N with FID detector.

Imines substrates were prepared according to the previously described procedure.¹³ Commercial 2-methylquinoline was purified by Kugelrohr distillation. Commercial 2-phenylquinoline was purified *via* flash chromatography (silica gel, hexanes/EtOAc).

Synthesis of CNN pincer ligand

6-Phenylpicolinaldehyde. A 250 mL round-bottom flask equipped with reflux condenser was charged with 10.0 g (53.8 mmol, 1 equiv.) of 6-bromopicolinaldehyde, 1.24 g (1.08 mmol, 0.02 equiv.) of Pd(PPh₃)₄ and 70 mL of degassed toluene. The reaction vessel was flushed with N₂. A separate solution of 9.83 g (80.6 mmol, 1.50 equiv.) of phenylboronic acid in 35 mL of degassed MeOH was added to the reaction mixture, followed by 54 mL of degassed Na₂CO₃ 2 M aqueous solution (108 mol, 2.0 equiv.). The resulting suspension was stirred at reflux for 16 h. After cooling to room temperature, the biphasic mixture was diluted with 200 mL of Na₂CO₃ 2 M aqueous solution and 100 mL of toluene, the phases were separated, and the aqueous layer was re-extracted with 100 mL of toluene followed by 2 × 100 mL of CH₂Cl₂. The combined organic layer was dried with MgSO₄ and concentrated under

reduced pressure. The resulting crude was purified *via* flash chromatography (silica gel, cyclohexane–CH₂Cl₂ 6 : 4), providing 9.51 g of the desired intermediate as yellowish oil (97% yield). ¹H NMR (400 MHz, CDCl₃): δ 10.18 (d, *J* = 0.6 Hz, 1H), 8.12–8.07 (m, 2H), 7.99–7.88 (m, 3H), 7.56–7.44 (m, 3H) ppm.

(*R*)-4-Isopropyl-2-(6-phenylpyridin-2-yl)-4,5-dihydrooxazole (ligand 1). A 500 mL round-bottom flask was charged with 9.50 g of the previous intermediate (51.9 mmol, 1 equiv.), 5.88 g of D-valine (57.0 mmol, 1.10 equiv.) and 250 mL of toluene. The reaction vessel was flushed with N₂ and stirred at room temperature for 2 h. 21.50 g of K₂CO₃ (155.6 mmol, 3.0 equiv.) and 26.32 g of I₂ (103.7 mmol, 2.0 equiv.) were charged as solids, the reaction vessel was flushed again with N₂ and stirred at 70 °C for 16 h. After cooling to room temperature, 250 mL of saturated Na₂SO₃ aqueous solution was added slowly and stirred for 10 min, with the complete disappearance of iodine color. The phases were separated and the aqueous layer was re-extracted with 3 × 200 mL of CH₂Cl₂. The combined organic layer was washed with brine, dried with MgSO₄ and concentrated under reduced pressure. The resulting crude was purified *via* flash chromatography (silica gel, cyclohexane with 2% Et₃N–EtOAc 85 : 15), providing 11.77 g of the desired ligand as white solid (85% yield). ¹H NMR (400 MHz, CDCl₃): δ 8.01–8.07 (m, 3H), 7.87–7.79 (m, 2H), 7.51–7.38 (m, 3H), 4.55 (dd, *J* = 9.6, 8.2 Hz, 1H), 4.26 (t, *J* = 8.3 Hz, 1H), 4.22–4.14 (m, 1H), 1.99–1.85 (m, 1H), 1.08 (d, *J* = 6.7 Hz, 3H), 0.96 (d, *J* = 6.8 Hz, 3H) ppm.

Synthesis of octahedral Ir(III) complexes

4-BArF. An oven-dried Schlenk flask was charged with 100 mg (65.7 mmol, 1 equiv.) of Crabtree's catalyst BArF analogue, followed by 17.5 mg (65.7 mmol, 1.0 equiv.) of ligand **1**. After purging with vacuum-nitrogen cycles, 2 mL of degassed THF was added and stirred until dissolution. Hydrogen from a balloon was bubbled into the solution through a needle for 10 minutes, and then the reaction mixture was stirred at room temperature for 1 h. The solvent was removed under reduced pressure and the resulting crude was purified *via* silica gel chromatography (cyclohexane–CH₂Cl₂ 5 : 5) collecting the bright orange band, providing 95 mg of the desired complex as orange solid (86% yield). ¹H NMR (400 MHz, CDCl₃): δ 8.33–8.26 (m, 2H), 8.00 (t, *J* = 7.8 Hz, 1H), 7.91 (dd, *J* = 7.7, 1.5 Hz, 1H), 7.79–7.74 (m, 2H), 7.71 (s, 8H), 7.51 (s, 4H), 7.46 (t, *J* = 7.5 Hz, 1H), 7.32 (t, *J* = 7.9 Hz, 2H), 7.20–7.10 (m, 4H), 4.71 (t, *J* = 10.4 Hz, 1H), 4.50 (t, *J* = 9.3 Hz, 1H), 4.21–4.12 (m, 1H), 2.21–2.08 (m, 1H), 1.86–0.66 (m, 33H), 0.84 (d, *J* = 7.1 Hz, 3H), 0.10 (d, *J* = 6.7 Hz, 3H), –21.00 (dd, *J* = 23.1, 8.2 Hz, 1H), –24.13 (dd, *J* = 23.7, 8.2 Hz, 1H) ppm. ¹³C NMR (101 MHz, CDCl₃): δ 171.2, 165.1, 161.8 (q, *J* = 49.8 Hz), 154.6, 146.0, 139.8, 138.9, 137.6, 134.9, 130.9, 130.1, 129.9, 129.0 (qq, *J* = 31.3, 3.0 Hz), 128.0, 126.4 (d, *J* = 2.5 Hz), 125.7, 124.7 (q, *J* = 272.7 Hz), 117.6, 72.1, 70.6, 35.8 (d, *J* = 31.3 Hz), 30.8, 29.9, 28.6 (d, *J* = 3.9 Hz), 27.6 (d, *J* = 11.1 Hz), 27.3 (d, *J* = 9.5 Hz), 27.1, 26.3, 19.8, 14.1 ppm. ³¹P NMR (162 MHz, CDCl₃): δ 14.79 (dd, *J* = 19.1, 4.1 Hz) ppm. ¹⁹F NMR (376 MHz, CDCl₃): δ –62.4 ppm. HRMS (ESI+, direct infusion): *m/z* [M–BArF]⁺ calcu-

lated for $[\text{C}_{40}\text{H}_{58}\text{IrN}_3\text{OP}]^+$: 820.3941, found 820.3953. IR-ATR (cm^{-1}): 2928, 2853, 1351, 1273, 1124, 885.

4-OTf. An oven-dried Schlenk flask was charged with 150 mg (185.4 mmol, 1 equiv.) of Crabtree's catalyst OTf analogue, followed by 49.4 mg (185.4 mmol, 1.0 equiv.) of ligand **1**. After purging with vacuum-nitrogen cycles, 2 mL of degassed THF was added and stirred until dissolution. Hydrogen from a balloon was bubbled into the solution through a needle for 10 minutes, and then the reaction mixture was stirred at room temperature for 1 h. The solvent was removed under reduced pressure and the resulting crude was purified *via* silica gel chromatography (CH_2Cl_2 -THF 9:1) collecting the bright orange band, providing 116 mg of the desired complex as orange solid (65% yield). ^1H NMR (400 MHz, CDCl_3): δ 8.44–8.36 (m, 3H), 8.29 (dd, J = 7.8, 1.4 Hz, 1H), 7.89–7.93 (m, 2H), 7.39–7.45 (m, 1H), 7.37–7.32 (m, 2H), 7.30 (dd, J = 8.3, 7.2 Hz, 2H), 7.15–7.09 (m, 2H), 4.83 (dd, J = 10.4, 9.2 Hz, 1H), 4.69 (t, J = 9.1 Hz, 1H), 4.15 (ddd, J = 10.3, 8.8, 3.7 Hz, 1H), 2.16 (m, 1H), 1.80–0.67 (m, 33H), 0.87 (d, J = 7.1 Hz, 3H), 0.21 (d, J = 6.7 Hz, 3H), –21.16 (dd, J = 23.2, 8.2 Hz, 1H), –24.03 (dd, J = 23.6, 8.2 Hz, 1H) ppm. ^{13}C NMR (101 MHz, CDCl_3): δ 171.9, 164.5, 155.0, 146.0, 140.4, 140.0, 137.7, 131.0, 130.3, 129.5, 127.7, 127.0, 126.6 (d, J = 2.5 Hz), 121.1 (q, J = 320.9 Hz), 72.1, 70.9, 35.8 (d, J = 30.9 Hz), 30.8, 30.5, 28.7 (d, J = 3.9 Hz), 27.7 (d, J = 11.1 Hz), 27.4 (d, J = 9.4 Hz), 26.4, 20.1, 14.8 ppm. ^{31}P NMR (162 MHz, CDCl_3): δ 14.54 (dd, J = 20.1, 5.9 Hz) ppm. ^{19}F NMR (376 MHz, CDCl_3): δ –78.1 ppm. HRMS (ESI+, direct infusion): m/z $[\text{M}-\text{OTf}]^+$ calculated for $[\text{C}_{40}\text{H}_{58}\text{IrN}_3\text{OP}]^+$: 820.3941, found 820.3953. IR-ATR (cm^{-1}): 2922, 2848, 2225, 1588, 1444, 1426, 1262, 1220, 1146, 1031.

5-BArF. An oven-dried Schlenk flask was charged with 100 mg (65.7 mmol, 1 equiv.) of Crabtree's catalyst BArF analogue, followed by 17.5 mg (65.7 mmol, 1.0 equiv.) of ligand **1**. After purging with vacuum-nitrogen cycles, 2 mL of toluene was added and the solution was stirred for 10 min at room temperature. Hydrogen from a balloon was bubbled into the solution through a needle for 10 minutes, and then the reaction mixture was stirred at 100 °C for 16 h. After cooling to room temperature, the solvent was removed under reduced pressure and the resulting crude was purified *via* silica gel chromatography (cyclohexane- CH_2Cl_2 5:5) collecting the bright orange band, providing 84 mg of the desired complex as orange solid (77% yield). ^1H NMR (400 MHz, CDCl_3): δ 8.07–8.01 (m, 2H), 7.96 (d, J = 8.2 Hz, 1H), 7.82 (t, J = 8.2 Hz, 1H), 7.72 (s, 8H), 7.62 (d, J = 7.3 Hz, 1H), 7.57 (tt, J = 7.7, 1.5 Hz, 1H), 7.52 (s, 4H), 7.51–7.49 (m, 1H), 7.39–7.34 (m, 1H), 7.03–6.95 (m, 4H), 4.70 (t, J = 9.9 Hz, 1H), 4.52 (dd, J = 9.5, 6.8 Hz, 1H), 4.6 (m, 1H), 2.11–0.81 (m, 34H), 0.79 (d, J = 7.0 Hz, 3H), 0.01 (d, J = 6.8 Hz, 3H), –13.86 (d, J = 26.2 Hz, 1H) ppm. ^{13}C NMR (101 MHz, CDCl_3): δ 172.8, 167.4, 161.9 (q, J = 49.8 Hz), 153.1, 144.6, 143.4, 141.7 (d, J = 7.6 Hz), 140.6, 139.3, 137.9, 134.9, 132.7, 129.0 (qq, J = 31.3, 2.9 Hz), 128.7, 126.3 (d, J = 2.5 Hz), 125.5, 124.7 (q, J = 273.7 Hz), 122.8, 121.1 (d, J = 4.9 Hz), 117.6, 71.2, 70.8, 35.7, 30.9, 29.7, 27.6, 27.1, 26.6, 19.3, 14.2 ppm. ^{31}P NMR (162 MHz, CDCl_3): δ 1.86 ppm. ^{19}F NMR (376 MHz, CDCl_3): δ –62.4 ppm. HRMS (ESI+, direct infusion):

m/z $[\text{M}-\text{BArF}]^+$ calculated for $[\text{C}_{40}\text{H}_{56}\text{IrN}_3\text{OP}]^+$: 818.3785, found 818.3776; IR-ATR (cm^{-1}): 2932, 2853, 1353, 1273, 1116, 885.

5-OTf. An oven-dried Schlenk flask was charged with 184 mg (227.4 mmol, 1 equiv.) of Crabtree's catalyst BArF analogue, followed by 60.6 mg (227.4 mmol, 1.0 equiv.) of ligand **1**. After purging with vacuum-nitrogen cycles, 5 mL of toluene was added and the suspension was stirred for 10 min at room temperature. Hydrogen from a balloon was bubbled into the solution through a needle for 10 minutes, and then the reaction mixture was stirred at 100 °C for 16 h. After cooling to room temperature, the solvent was removed under reduced pressure and the resulting crude was purified *via* silica gel chromatography (CH_2Cl_2 -THF 9:1) collecting the bright orange band, providing 130 mg of the desired complex as orange solid (62% yield). ^1H NMR (400 MHz, CDCl_3): δ 8.20–8.12 (m, 2H), 8.08–8.00 (m, 2H), 7.64 (tt, J = 7.6, 1.5 Hz, 1H), 7.56–7.51 (m, 1H), 7.41–7.36 (m, 1H), 7.14 (t, J = 6.7 Hz, 1H), 7.02–6.93 (m, 2H), 4.86 (dd, J = 10.2, 9.4 Hz, 1H), 4.76 (dd, J = 9.4, 7.2 Hz, 1H), 4.04 (ddd, J = 10.1, 7.2, 4.4 Hz, 1H), 2.08–0.86 (m, 34H), 0.84 (d, J = 7.0 Hz, 3H), 0.18 (d, J = 6.7 Hz, 3H), –13.96 (d, J = 26.2 Hz, 1H) ppm. ^{13}C NMR (101 MHz, CDCl_3): δ 173.4, 166.8, 153.3, 144.7, 144.1, 141.8 (d, J = 7.6 Hz), 140.4, 140.2, 137.9, 132.2, 129.1, 127.0, 126.5 (d, J = 2.6 Hz), 125.3, 122.6, 122.2 (q, J = 323.2 Hz), 121.5, 71.8, 70.8, 35.4, 31.3, 29.2, 27.7, 26.7, 19.5, 15.2 ppm. ^{31}P NMR (162 MHz, CDCl_3): δ 1.47 ppm. ^{19}F NMR (376 MHz, CDCl_3): δ –78.1 ppm. HRMS (ESI+, direct infusion): m/z $[\text{M}-\text{OTf}]^+$ calculated for $[\text{C}_{40}\text{H}_{56}\text{IrN}_3\text{OP}]^+$: 818.3785, found 818.3800. IR-ATR (cm^{-1}): 2926, 2850, 2238, 2136, 1571, 1446, 1258, 1148, 1029, 915.

6-OTf. A round-bottom flask equipped with compact distillation apparatus was charged with 150 mg (155.1 mmol) of complex **5-OTf** and 25 mL of acetonitrile. After purging the system with N_2 , the solvent was distilled at atmospheric pressure until almost dryness, and 25 mL of fresh acetonitrile was added. The stripping cycle was repeated 2 additional times to distil a total of approximately 3×25 mL of solvent. The final solution was concentrated under reduced pressure, and the crude was purified *via* silica gel chromatography (CH_2Cl_2 - CH_3CN 9:1) collecting the bright orange band, providing 111 mg of the desired complex as orange solid (92% purity, 71% yield). ^1H NMR (400 MHz, CD_3CN): δ 8.14 (d, J = 8.3 Hz, 1H), 8.05 (t, J = 7.9 Hz, 1H), 7.79 (d, J = 7.5 Hz, 1H), 7.76–7.66 (m, 1H), 7.40–7.32 (m, 1H), 7.11–7.01 (m, 1H), 4.92 (t, J = 9.8 Hz, 1H), 4.82 (dd, J = 9.4, 5.8 Hz, 1H), 4.13 (ddd, J = 9.6, 5.8, 3.2 Hz, 1H), 1.85–0.90 (m, 34H), 1.03 (d, J = 7.0 Hz, 3H), 0.86 (d, J = 6.7 Hz, 3H), –15.24 (d, J = 25.4 Hz, 1H) ppm. ^{13}C NMR (101 MHz, CD_3CN): δ 173.6, 167.7, 146.2, 145.6, 142.3, 140.6, 139.1 (d, J = 8.1 Hz), 132.4, 126.0, 123.4, 122.2 (d, J = 14.5 Hz), 72.5, 70.8, 35.3, 31.7, 29.5, 28.0, 27.3 (d, J = 1.4 Hz), 19.3, 15.6 ppm. ^{31}P NMR (162 MHz, CD_3CN): δ 2.92 (d, J = 6.8 Hz) ppm. ^{19}F NMR (376 MHz, CD_3CN): δ –79.3 ppm. HRMS (ESI+, direct infusion): m/z $[\text{M}-\text{OTf}-\text{CH}_3\text{CN}]^+$ calculated for $[\text{C}_{35}\text{H}_{51}\text{IrN}_2\text{OP}]^+$: 739.3363, found 739.3325; m/z $[\text{M}-\text{OTf}-\text{CH}_3\text{CN}-2\text{H}]^+$ calculated for $[\text{C}_{35}\text{H}_{49}\text{IrN}_2\text{OP}]^+$: 737.3206, found 737.3230. IR-ATR (cm^{-1}): 2924, 2850, 2125, 1575, 1148, 1258, 1146, 1029.

Asymmetric hydrogenation of imines and quinolines

2.0 mg of catalyst (0.01 equiv.), substrate (1 equiv.) and 1 mL of anhydrous CH_2Cl_2 were placed in a glass tube inside a hydrogenation reactor. After purging with vacuum-nitrogen-hydrogen cycles, the system was adjusted to 3 bar of hydrogen. After stirring at room temperature for 14–20 h, the pressure was released and the solvent was removed under reduced pressure. Conversions were determined *via* ^1H -NMR of the reaction crude and enantiomeric excesses were determined *via* chiral HPLC/GC analysis.

Data availability

The data supporting this article have been included as part of the ESI.† Crystallographic data for complexes **4-BArF** and **5-BArF** have been deposited at the Cambridge Crystallographic Data Centre under CCDC 2430455 and 2430460,† respectively.

Conflicts of interest

The authors declare no conflict of interest.

Acknowledgements

This work was supported by a grant to A. R. and X. V. from Ministerio de Ciencia, Innovación y Universidades (PID2023-147298NB-I00 funded by MCIU/AEI/10.13039/501100011033/FEDER, UE). IRB Barcelona is the recipient of institutional funding from MICINN through the Centres of Excellence Severo Ochoa Award and from the CERCA Program of the Catalan Government. We thank Generalitat de Catalunya for grant 2021 SGR 00866. Y. W. thanks MICINN for a predoctoral fellowship.

References

- G. Q. Lin, J. G. Zhang and J. F. Cheng, in *Chiral Drugs: Chemistry and Biological Action*, 2011, pp. 3–28.
- A. Baeza and A. Pfaltz, *Chem. – Eur. J.*, 2010, **16**, 4003–4009.
- A. Cabré, X. Verdager and A. Riera, *Chem. Rev.*, 2022, **122**, 269–339.
- A. N. Kim and B. M. Stoltz, *ACS Catal.*, 2020, **10**, 13834–13851.
- J. J. Verendel, O. Pàmies, M. Diéguez and P. G. Andersson, *Chem. Rev.*, 2014, **114**, 2130–2169.
- S. F. Zhu and Q. L. Zhou, *Acc. Chem. Res.*, 2017, **50**, 988–1001.
- C. Margarita and P. G. Andersson, *J. Am. Chem. Soc.*, 2017, **139**, 1346–1356.
- E. Salomó, S. Orgué, A. Riera and X. Verdager, *Angew. Chem., Int. Ed.*, 2016, **55**, 7988–7992.
- A. Cabré, E. Romagnoli, P. Martínez-Balart, X. Verdager and A. Riera, *Org. Lett.*, 2019, **21**, 9709–9713.
- M. Biosca, P. de la Cruz-Sánchez, J. Faiges, J. Margalef, E. Salomó, A. Riera, X. Verdager, J. Ferré, F. Maseras, M. Besora, O. Pàmies and M. Diéguez, *ACS Catal.*, 2023, **13**, 3020–3035.
- M. Biosca, E. Salomó, P. De La Cruz-Sánchez, A. Riera, X. Verdager, O. Pàmies and M. Diéguez, *Org. Lett.*, 2019, **21**, 807–811.
- E. Salomó, A. Gallen, G. Sciortino, G. Ujaque, A. Grabulosa, A. Lledós, A. Riera and X. Verdager, *J. Am. Chem. Soc.*, 2018, **140**, 16967–16970.
- Y. Wen, M. Fernández-Sabaté, A. Lledós, G. Sciortino, J. Eills, I. Marco-Rius, A. Riera and X. Verdager, *Angew. Chem., Int. Ed.*, 2024, **63**, e202404955.
- J. Choi, A. H. R. MacArthur, M. Brookhart and A. S. Goldman, *Chem. Rev.*, 2011, **111**, 1761–1779.
- M. Gupta, C. Hagen, R. J. Flesher, W. C. Kaska and C. M. Jensen, *Chem. Commun.*, 1996, **36**, 2083–2084.
- P. Paredes, J. Díez and M. P. Gamasa, *Organometallics*, 2008, **27**, 2597–2607.
- C. P. Owens, A. Varela-Álvarez, V. Boyarskikh, D. G. Musaev, H. M. L. Davies and S. B. Blakey, *Chem. Sci.*, 2013, **4**, 2590–2596.
- L. Qian, X. Tang, Z. Huang, Y. Wang, G. Liu and Z. Huang, *Org. Lett.*, 2021, **23**, 8978–8983.
- L. Qian, X. Tang, Y. Wang, G. Liu and Z. Huang, *Chin. J. Chem.*, 2022, **40**, 1131–1136.
- L. Qian, C. Yu, L. Gan, X. Tang, Y. Wang, G. Liu, X. Leng, Z. Sun, Y. Guo, X. S. Xue and Z. Huang, *J. Am. Chem. Soc.*, 2024, **146**, 3427–3437.
- M. P. Jensen, S. J. Lange, M. P. Mehn, E. L. Que and L. Que, *J. Am. Chem. Soc.*, 2003, **125**, 2113–2128.
- T. Wang, X. Q. Hao, J. J. Huang, K. Wang, J. F. Gong and M. P. Song, *Organometallics*, 2014, **33**, 194–205.
- We believe the remaining 8% corresponds to an isomer of **6-OTf** with a hydride peak at -23.46 ppm (d, $J = 20.6$ Hz). The mixture provides a single peak by HRMS.
- For steric and electronic reasons, we believe that hydrogen is a better ligand at the iridium reactive site and thus no major product inhibition was observed.
- T. Wang, L. G. Zhuo, Z. Li, F. Chen, Z. Ding, Y. He, Q. H. Fan, J. Xiang, Z. X. Yu and A. S. C. Chan, *J. Am. Chem. Soc.*, 2011, **133**, 9878–9891.
- B. Tutkowski, S. Kerdphon, E. Limé, P. Helquist, P. G. Andersson, O. Wiest and P. O. Norrby, *ACS Catal.*, 2018, **8**, 615–623.
- G. E. Dobereiner, A. Nova, N. D. Schley, N. Hazari, S. J. Miller, O. Eisenstein and R. H. Crabtree, *J. Am. Chem. Soc.*, 2011, **133**, 7547–7562.